



Shape memory properties and microstructure evolution of Cu–Al–Fe alloys with different Fe contents

Hongyu Wang^{1,a)} , Jianchao Feng¹, Sheng Chen¹, Xiaoming Yuan¹, Duo Xu¹

¹School of Mechanical Engineering, Jiangsu University, Zhenjiang 212013, Jiangsu, China

^{a)}Address all correspondence to this author. e-mail: ujswhy2020@163.com

Received: 1 June 2023; accepted: 19 October 2023; published online: 31 October 2023

(87 – x)Cu–13Al–xFe (x: 1, 2, 3, 4, 5 wt%) alloys were prepared by arc melting deposition process. Results showed that with the increase of Fe content, the memory recovery ratio of (87 – x)Cu–13Al–xFe alloy showed a three-phase change of decrease–increase–decrease under 4% pre-strain. The memory recovery ratio of the 4Fe alloy reached 100%. The analysis shows that a Fe-rich κ phase is formed when the Fe content exceeds its solubility in the Cu–Al alloy. The κ -phase not only shifts the eutectoid point of the alloy to the right and refines the grain size but also has a “pinning” effect. This effect flattens the grain boundaries of the alloy, elongates the grains, and increases the order degree of the martensite, thereby improving its shape memory properties. However, when the Fe content is too high, the alloy will enter a sub-eutectic state, leading to the coexistence of two-phase martensite and reducing the shape memory properties of the alloy.

Introduction

Cu–Al alloys have attracted considerable attention among Cu-based shape memory alloys (SMAs) due to their excellent shape memory effect (SME), wide temperature range of phase transition, and high electrical and thermal conductivity [1–3]. However, the mechanical properties of Cu–Al SMAs are poor due to their polycrystalline brittleness and anisotropy and their shape memory properties cannot be fully utilized due to brittle failure during operation [4, 5]. For Cu–Al SMAs, in order to have good SME, the Al content is generally between 12 and 16 wt%, but the brittleness of the alloy increases sharply when the Al content exceeds 11.5 wt% [6]. It can be assumed that there is a conflict between the SME and brittleness in Cu–Al SMAs. To address the brittleness problem of the alloys, Ueland et al. proposed the development of the alloys toward oligocrystalline and monocrystalline structures [7], and some researchers have focused on the introduction of third-phase elements to develop Cu–Al–X SMAs (X: Ni, Be, Mn, etc.) [8–10]. However, in the research of shape memory alloys, scholars usually use the method of elemental addition to modulate the alloy properties [11, 12]. However, the problem of brittleness of Cu–Al–Ni alloys is still prominent [13]. The Be element used in Cu–Al–Be shape memory alloys is expensive and highly toxic, while the thermal

stability of Cu–Al–Mn SMAs is relatively poor [14]. In recent years, researchers have tried to introduce Fe as a third-phase element to improve the properties of Cu–Al SMAs [15–17]. The addition of Fe element not only has a positive effect on improving the brittleness of Cu–Al SMAs, but also performs well in improving the SME of the alloys. For example, Raju et al. [18] prepared Cu–Al–Fe SMAs with different Fe contents by casting method, and the shape recovery ratio of Cu–12.08Al–2.89Fe alloy reached 94% when the pre-strain was 5%. However, the existing researches only focus on the changes in the properties of Cu–Al SMAs after the introduction of Fe, while the study of the mechanism of Fe, especially its mechanism on the SME of Cu–Al SMAs, is extremely rare.

In this study, Cu–Al–Fe SMAs with different Fe contents were designed based on the Cu–Al binary alloy phase diagram, the alloy was fabricated by arc additive manufacturing, and the alloy SME was measured by the bending deformation method. The microstructure of the alloy in the deposited and quenched state was analyzed by optical microscopy (OM). The aim was to establish the relationship between the microstructure evolution and the memory properties of Cu–Al–Fe alloys and to clarify the mechanism of Fe introduction on the memory properties of Cu–Al alloys.

Results and analysis

Shape memory properties of Cu–Al–Fe alloys

As shown in Fig. 1, the memory recovery ratio of Cu–Al–Fe alloys shows a three-phase change of decrease–increase–decrease with increasing Fe content. At 4% pre-strain, the 2Fe alloy has the lowest MR ratio of only 77.9%, while the 4Fe alloy recovers completely. Cu–Al-based SMAs themselves have good shape memory properties. For example, Wang et al. [19] prepared a Cu–Al–Mn alloy that could achieve a memory recovery ratio of 84.4% under 6% pre-strain. The introduction of Fe into the Cu–Al-based SMAs can further improve their shape memory

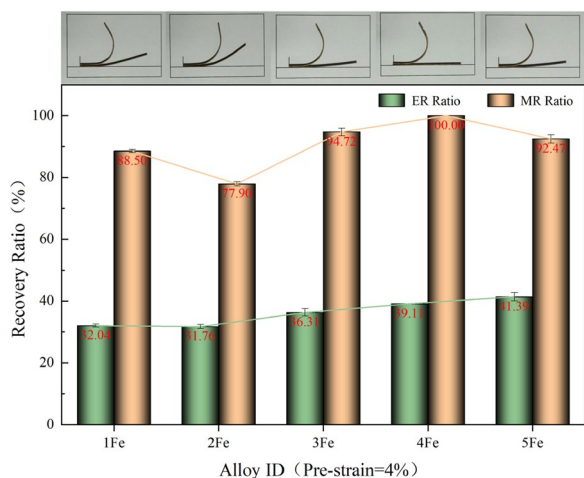


Figure 1: Elastic recovery ratio and memory recovery ratio of Cu–13Al–xFe ($x = 1, 2, 3, 4, 5$) alloys and related physical pictures.

recovery ratio, indicating that the introduction of Fe is beneficial for improving the memory properties of the alloy. Meanwhile, with the increase of Fe content, the ER ratio of Cu–Al–Fe alloys generally shows an increasing trend, increasing from about 32% in 1Fe and 2Fe alloys to 41.39% in the 5Fe alloy. No macroscopic cracks were found in any of the Cu–Al–Fe alloy specimens prepared by 180° cold bending, indicating that the introduction of Fe into Cu–Al alloys also has a positive effect on improving their brittleness.

As-deposited microstructures

Figure 2 shows the metallographic microstructure images of Cu–Al–Fe alloys with different Fe contents in the as-deposited state.

As shown in Fig. 2, the as-deposited microstructure of the 1Fe alloy consists of a gray matrix with a plum-shaped precipitate. Combined with the Cu–Al binary phase diagram shown in Fig. 1 and the Cu–Al–Fe ternary phase diagram shown in Fig. 3, the gray matrix can be identified as an $\alpha + \gamma^2$ eutectoid, and the plum-shaped precipitate can be identified as a γ^2 (Cu_9Al_4) phase. γ^2 is distributed both inside and at the grain boundary of the crystal. No complete grains can be observed at 200× magnification. When the magnification is reduced to 50× [Fig. 2(f)], the as-deposited microstructure of the 1Fe alloy will show a cell-like shape with smooth grain boundaries, and the grain size is in the millimeter range. In the 2Fe alloy, the as-deposited microstructure of the alloy consists of gray matrix with floc-like precipitates having the

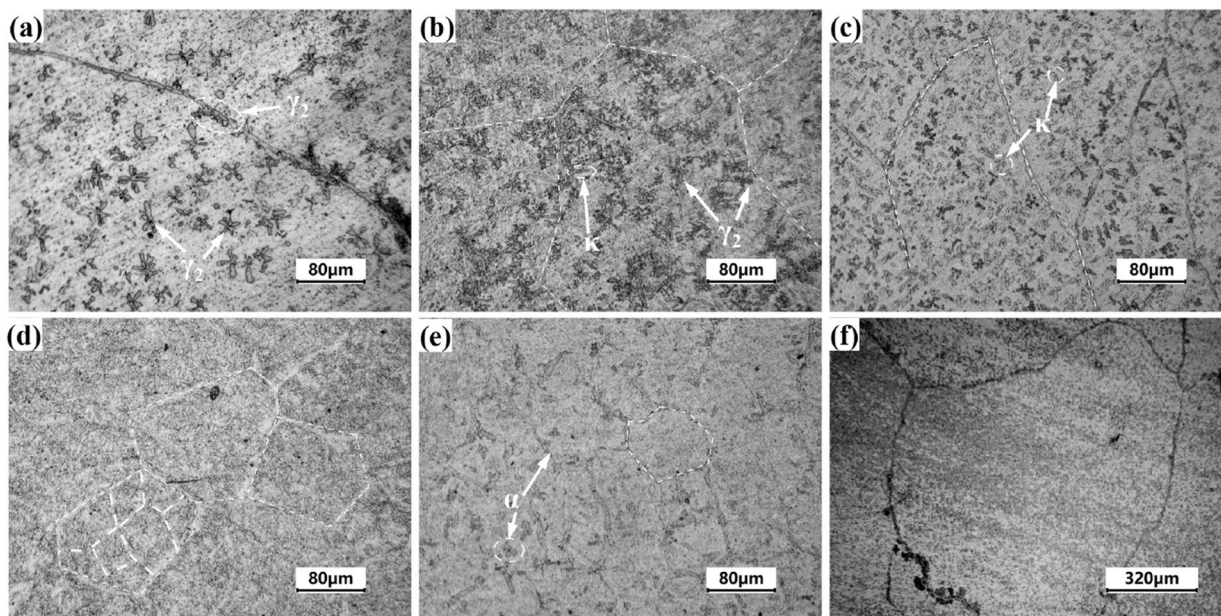


Figure 2: As-deposited microstructure of Cu–Al–Fe alloys with different Fe contents. (a) 1-wt% Fe; (b) 2-wt% Fe; (c) 3-wt% Fe; (d) 4-wt% Fe; (e) 5 wt%; and (f) 1 wt% (50×).

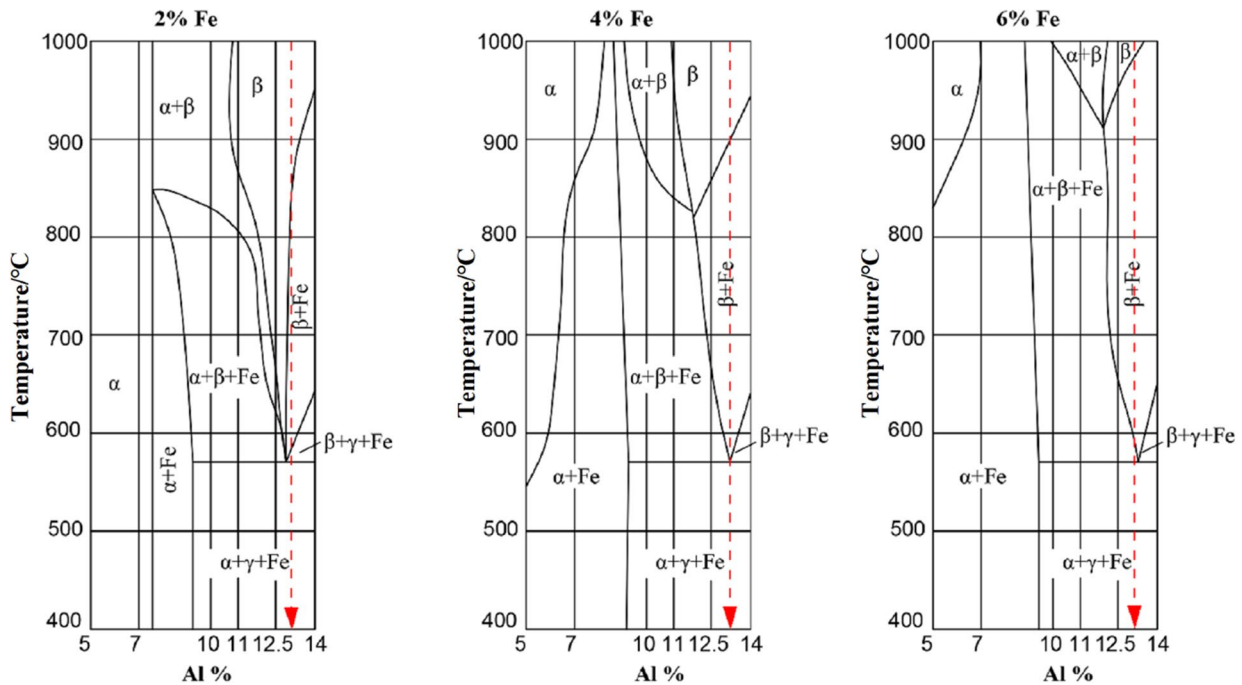


Figure 3: Phase equilibrium of Cu–Al–Fe system.

same color as the γ^2 phase. As the Fe content increases, the eutectic point of the Cu–Al alloy shifts to the right, resulting in a decrease in the precipitation of the γ^2 phase. According to the Cu–Al–Fe ternary phase diagram in Fig. 3, the 2Fe alloy is still a hyper-eutectic alloy, so it is concluded that these floc-like precipitates are still γ^2 phase. The change of γ^2 phase from plum like to floc like is due to the thinning and reduction of the γ^2 phase bar-shaped petals. In addition, gray grain-like precipitates can be observed both at the grain boundaries and in the floc-like γ^2 phase. Since the solubility of Fe in Cu–Al alloy is limited, Fe and Al will form a Fe-rich Fe–Al compound when the Fe content exceeds its solubility. It can be inferred that these gray granular precipitates are κ (Fe_3Al) phase, which is the Fe phase in the Cu–Al–Fe ternary phase diagram as shown in Fig. 3. Complete grains with a size of about 500 μm can be found under the 400-fold view. In the 3Fe alloy, the as-deposited microstructure of the 3Fe alloy shows a decreasing number of γ^2 phase and an increasing amount of gray κ phase. The grain size of the 3Fe alloy does not change significantly from that of the 2Fe alloy, but the grain shape changes from regular polygons to elongated shapes with pointed ends. In the 4Fe alloy, the γ^2 phase has completely disappeared, which is consistent with the Cu–Al–Fe ternary phase diagram shown in Fig. 3, indicating that the 4Fe alloy is almost at the eutectic point. In the 5Fe alloy, the white precipitate appears at the grain boundaries of the alloy. Combined with the ternary phase diagram of Cu–Al–Fe shown in Fig. 3, the 5Fe alloy is a sub-eutectic alloy, which can be inferred to be an α -phase.

With the increase of Fe content, the deposited microstructure of Cu–Al–Fe alloy shows the following three changes. First, the precipitation of γ^2 phase in the deposited microstructure of Cu–Al–Fe alloy gradually decreases until it disappears, while the precipitation of Fe-rich κ phase increases. When the amount of κ phase reaches saturation, the α phase is influenced by the κ phase and transforms into a globular shape. This change is directly related to the evolution of the Cu–Al–Fe alloy. With increasing Fe content, the microstructure in the deposited state changes from hyper-eutectic to near-eutectic and finally to sub-eutectic. Secondly, the grain size of the deposited microstructure of the Cu–Al–Fe alloy becomes small, decreasing from millimeters in the 1Fe alloy to hundreds of micrometers in the 2Fe, 3Fe, and 4Fe alloys and then to tens of micrometers in the 5Fe alloy. The analysis suggests that the refinement of the alloy grains is related to the formation of a new phase, the κ -phase, after the introduction of Fe. With increasing Fe content, the amount of κ phase in the Cu–Al–Fe alloy continuously increases. The κ -phase acts as a nucleus of heterogeneous nuclei that refine the alloy grains. Third, the grain shape of the deposited state of the Cu–Al–Fe alloy undergoes a transformation from a cellular shape with smooth grain boundaries (1Fe alloy) to a regular polygon with straight grain boundaries (2Fe alloy), then to a willowy shape with pointed and elongated ends (3Fe alloy), and then back to a polygon with straight grain boundaries (4Fe alloy) and a cellular shape with smooth grain boundaries (5Fe alloy).

The results show that the introduction of Fe into Cu–Al SMAs not only shifts the eutectic point of the alloy to the right,

but also has the effect of refining its grains and influencing the shape of its grain boundaries.

Quenched microstructure

Figure 4 shows the metallographic microstructure of different Fe-containing Cu–Al–Fe alloys in quenched state.

As shown in Fig. 4, the quenched microstructure of the 1Fe alloy consists of a plate-like martensite and numerous black dot-like precipitates. The 1Fe alloy is a hypereutectoid alloy that precipitates γ^2 phase during quenching, so the black dot-like precipitates are γ^2 phase. The γ^2 phase is a hard phase that makes the alloy hard and brittle. The presence of the γ^2 phase inhibits the growth of martensite in the 1Fe alloy during quenching, resulting in a more pronounced martensitic crossover phenomenon. In addition, the grain size and shape of the quenched microstructure of the 1Fe alloy are basically the same as those of the deposited microstructure. In the 2Fe alloy, the quenched microstructure still consists of a plate-like martensite and black dot-like γ^2 phase, but the amount of γ^2 phase is less than that of 1Fe alloy, and the martensite intersection phenomenon is more severe than that of 1Fe alloy. The grain size of the quenched microstructure of 2Fe alloy is basically the same as that of the deposited microstructure, but the shape has changed from regular polygons to irregular polygons with more prominent corners. Combined with the analysis of the deposited microstructure, the changes in the quenched microstructure of the 2Fe alloy are considered to be related to the formation of a new phase κ phase. In the 3Fe alloy, the microstructure of the alloy is mainly

composed of a single plate-like martensite. Compared with the 2Fe alloy, the martensite intersection phenomenon in 3Fe alloy has been improved and the martensite order is better. The grain size of the quenched microstructure of the 3Fe alloy is basically the same as that of the deposited microstructure, but the shape is no longer lancet shaped and the grain boundaries have become flatter. In the 4Fe alloy, martensite is better ordered compared to the 3Fe alloy. The grain size of the quenched microstructure of 4Fe alloy is larger than that of the deposited microstructure, and the shape has become lancet shaped. This change is attributed to the substructure promoted by the κ phase in the deposited microstructure of the 4Fe alloy. The quenched microstructure of 5Fe alloy consists of gray cellular crystals mixed with white blocky structure. The martensite in the quenched microstructure of 5Fe alloy has higher order and smaller lath spacing, and the grain size and shape are basically consistent with those of its deposited microstructure, except for the relatively smaller size of the white blocky structure.

From Figs. 6 and 7, it can be seen that the quenched microstructure of Cu–Al–Fe alloys with different Fe contents shows good inheritance in terms of microstructure composition and grain size compared with their deposited microstructure, but the orderliness and grain morphology of the formed martensite do not continue. For example, severe martensite intersection phenomenon can be observed in the quenched microstructure of 2Fe alloy, and the grain morphology of the quenched microstructure in 3Fe and 4Fe alloys differs greatly from their deposited microstructure.

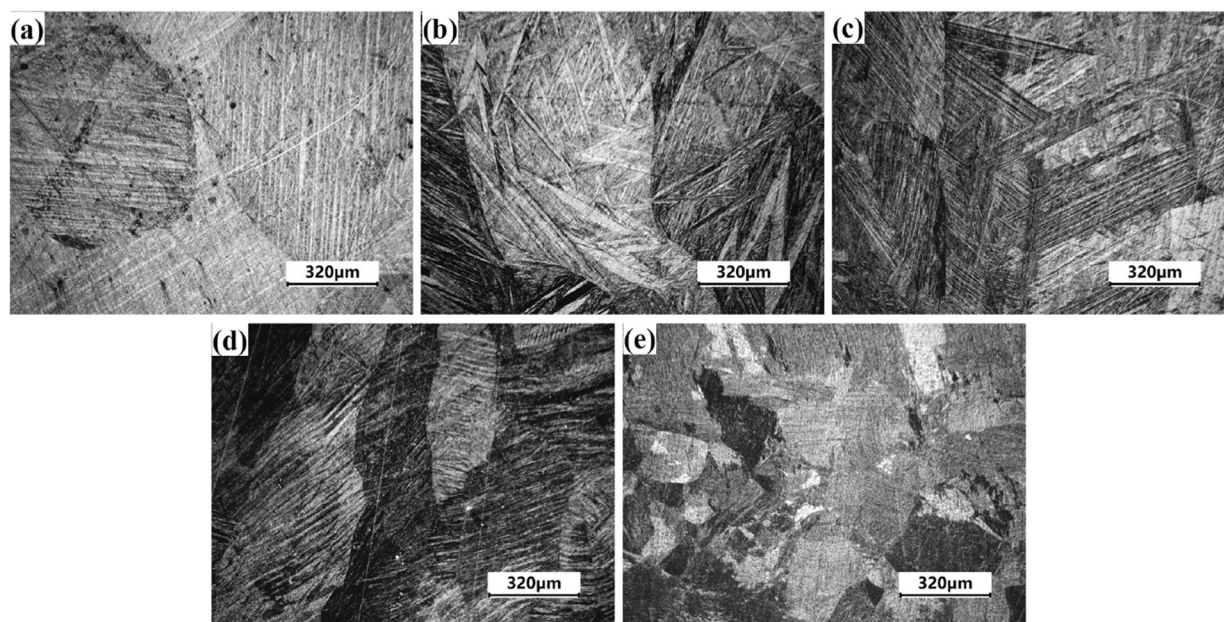


Figure 4: As-quenched microstructure of Cu–Al–Fe alloys with different Fe contents. (a) 1-wt% Fe; (b) 2-wt% Fe; (c) 3-wt% Fe; (d) 4-wt% Fe; and (e) 5 wt%.

Discussion

According to the above-mentioned shape memory properties and microstructure evolution of Cu–Al–Fe alloys with different Fe contents, it can be seen that the relationship between the shape memory properties of Cu–Al–Fe alloys with different Fe contents and their microstructures is generally consistent with the general mechanism of the shape memory effect of Cu–Al memory alloys, i.e., the more the quenched state organization of the alloy tends to be a single martensite, the higher the degree of martensite ordering, and the smaller the grain size of the alloy, the better the shape memory properties of the alloy.

For example, the 4Fe alloy studied in this paper has almost consistent martensite orientation in the quenched microstructure, with a grain size of about 200 μm in the width direction and composed of a single martensite [Fig. 4(d)]; correspondingly, its MR ratio reaches 100% under the set 4% pre-strain. The quenched microstructure of 5Fe alloy has higher martensitic orientation consistency, smaller lath spacing, and smaller grain size than that of 4Fe alloy [Fig. 4(e)], but its MR ratio drops to 92.47%, which is directly related to its quenched microstructure containing two types of martensite. The presence of a large amount of γ^2 phase in 3Fe alloy [Fig. 2(c)] leads to martensite intersection phenomenon in the quenched microstructure. A lower consistency of martensite orientation compared to 4Fe alloy, with larger grain size, resulting in a lower memory recovery ratio than 4Fe alloy, but higher than 5Fe alloy. The 1Fe alloy shows a similar situation to the 3Fe alloy. However, the Fe content in 2Fe alloy is higher than that in 1Fe alloy; according to the revealed effect of Fe on the eutectic point of Cu–Al alloy, the amount of γ^2 phase in 2Fe alloy is less compared to 1Fe alloy, which is also confirmed by the microstructure shown in [Fig. 2(b)]. However, the martensite orientation consistency in the quenched microstructure of 2Fe alloy is the poorest among all the prepared alloys, resulting in the lowest memory recovery ratio.

In addition, the grain size of the 2Fe alloy in both the deposited and quenched microstructure is smaller than that of the 1Fe alloy; however, the elastic recovery ratio of the 2Fe alloy is lower than that of the 1Fe alloy, which is not consistent with the general understanding of grain refinement strengthening. Overall, the change of Fe content from 1 to 2 wt% in Cu–Al–Fe alloy is a key point that deserves attention and further investigation.

The analysis shows that the κ phase is the key point that affects both alloys. The solubility of Fe in Cu–Al alloy is limited. If the Fe content exceeds its solubility, the excess Fe will react with Al to form Fe and Al compounds, namely κ phase. The κ phase will also cause some Al dissolved in Cu to be precipitated, which will actually reduce the concentration of Al in the Cu–Al alloy. This is the basic reason why the introduction of Fe will shift the eutectic point of Cu–Al alloy to the right. At the same

time, the κ phase is an ordered body-centered cubic lattice at room temperature, which mainly exists in a diffuse distribution and can act as a nucleus for heterogeneous nucleation during the solidification of the alloy [20]. This explains why the grain size of the alloy decreases continuously with increasing of Fe content.

In the 1Fe alloy, Fe is mainly in the form of solid solution and plays a strengthening role in the matrix and its influence on the eutectic point is not significant. The 1Fe alloy contains a large amount of γ^2 phase and its microstructure is almost the same as the Cu–Al alloy without Fe. However, it exhibits good elasticity, no macroscopic cracks are found after 180° bending under 4% pre-strain, and the ER ratio is about 32%. This is related to the strengthening effect of the matrix by the introduction of Fe. In other words, the memory properties of the 1Fe alloy are still mainly influenced by the γ^2 phase. In the 2Fe alloy, the Fe content exceeds its solubility in the Cu–Al alloy. On the one hand, the excess Fe will form new κ phase with Al. As the melting point of Fe (1538 °C) is higher than that of Cu (1085 °C), there will be a competitive relationship between them during the reaction and solidification process with Al, resulting in the morphological transition of γ^2 phase from the plum-shaped of 1Fe alloy to the cluster-like in the deposited microstructure of 2Fe alloy, and the formed κ phase will be mixed with the cluster-like morphology of γ^2 phase. On the other hand, due to the introduction of Fe, the solubility of Al in Cu–Al alloy will also decrease. The newly formed κ phase, constrained by the γ^2 phase, will not only be mixed with the cluster-like γ^2 phase, but also tend to aggregate toward the grain boundaries, which is more significant with the increase of Fe content. As shown in the deposited microstructures of 3Fe alloy and 4Fe alloy, this further confirms the above observations.

In addition, the grain boundaries of the deposited state of the 2Fe alloy are transformed from the smooth grain boundaries of the 1Fe alloy to flat regular polygons. The analysis shows that this is the role of the κ phase. The 2Fe alloy is close to the critical value for κ phase formation. The competition between Fe and Cu in the reaction and solidification process with Al, the aggregation tendency of κ phase toward grain boundaries, and especially the “pinning” effect of κ phase are all in a critical state and highly unstable, together with the martensite formation process for non-equilibrium transformation, the two together lead to the alloy after quenching martensite crossover phenomenon is serious. This explains the reason for the low recovery ratio of memory in 2Fe alloy. As for the decrease of ER ratio in 2Fe alloy compared to 1Fe alloy, it is also influenced by this factor.

Further observation of [Figs. 2(c) and (d) and 7(c) and (d)] shows that the grain shape in the deposition microstructure of 3Fe alloy is a pointed and elongated willow shape, indicating that the “pinning” effect of κ phase not only flattens the grain boundaries but also elongates the grains. This effect is also reflected in the quenched microstructures of 3Fe and 4Fe alloys, where

the grain boundaries of 3Fe alloy are flattened, while the grain shape of 4Fe alloy is elongated, further confirming the importance of the “pinning” effect of κ phase on the microstructure of Cu–Al–Fe alloy. The analysis shows that the reasons for the delayed “pinning” effect of κ phase in the quenched state microstructure compared to the deposition state microstructure are that quenching is a solid–solid-phase transformation process, while solidification is a liquid–solid-phase transformation process, which requires more force to achieve the effect. The pinning effect of the κ phase is also reflected in the martensitic orientation. As the Fe content increases, the amount of κ phase increases, and the constraint of κ phase dispersed in the crystal gradually weakens the martensitic crossover phenomenon.

Conclusion

- (1) With the increase of Fe content, the recovery ratio of memory of Cu–Al–Fe alloy shows a three-step variation, first decreasing, then increasing, and then decreasing again. The 4Fe alloy in the study exhibits a MR ratio of 100% under the set pre-strain of 4%. Meanwhile, the ER ratio of Cu–Al–Fe alloy shows an increasing trend with the increase of Fe content, from about 32.04% in 1Fe alloy to 41.39% in 5Fe alloy, among which the ER ratio of 4Fe alloy is 39.11%.
- (2) With the increase of Fe content, the precipitated microstructure of Cu–Al–Fe alloy shows three main changes. First, the γ^2 phase gradually decreases until it disappears, and at the same time, the κ phase gradually increases. When the κ phase reaches a saturation state, the α phase is affected and transformed into a bead-like shape. Second, the grain size becomes finer, decreasing from the millimeter scale in 1Fe alloy to several hundred microns in 2Fe, 3Fe, and 4Fe alloys and further decreasing to tens of microns in 5Fe alloy. Third, the grain shape undergoes a transition from the smooth cell-shaped grain boundaries in 1Fe alloy to the regular polygonal grain boundaries with flat surfaces in 2Fe alloy, then to the pointed and elongated willow shape in 3Fe alloy, and then back to the polygonal grain boundaries with flat surfaces in 4Fe alloy and the smooth cell-shaped grain boundaries in 5Fe alloy.
- (3) The quenched microstructure of Cu–Al–Fe alloy has better inheritability in terms of tissue composition and grain size compared to the depositional microstructure, but there is no continuity in terms of grain shape and the orderliness of the formed martensite.
- (4) After Fe is introduced into the Cu–Al alloy, when the Fe content exceeds its solubility in the alloy, a Fe-rich κ phase is formed. The formation of κ phase not only

shifts the eutectic point of the alloy to the right and refines the grain size, but also has a “pinning” effect. The “pinning” effect of the κ phase flattens the grain boundaries and elongates the grains, which improves the martensitic order of the alloy, thereby improving the shape memory properties of the alloy.

Materials and methods

Alloy composition design

In the Cu–Al shape memory alloy system, the Al content plays a crucial role in the memory properties of the alloy [21, 22]. According to the Cu–Al binary phase diagram shown in Fig. 5, when the Al content is less than 9.4 wt%, the microstructure of the alloy is completely composed of the α -phase at room temperature. At this point, the alloy has good plasticity and cold workability but no shape memory properties. When the Al content is above 15.6 wt%, the alloy consists entirely of the γ^2 phase (a copper-rich Cu–Al compound) at the eutectic temperature and is a two-phase mixture containing a large amount of the γ^2 phase at room temperature. The γ^2 phase is a hard phase, which makes the alloy hard and brittle and greatly weakens the shape memory recovery ability of the alloy. Therefore, in order to obtain better shape memory properties, the composition of the Cu–Al alloy is generally controlled near the eutectic point ($\omega(\text{Al}) = 11.8$ wt%). Considering that the introduction of Fe shifts the eutectic point of the Cu–Al alloy to the right [23], the Al content in the Cu–Al–Fe alloy in this study is determined

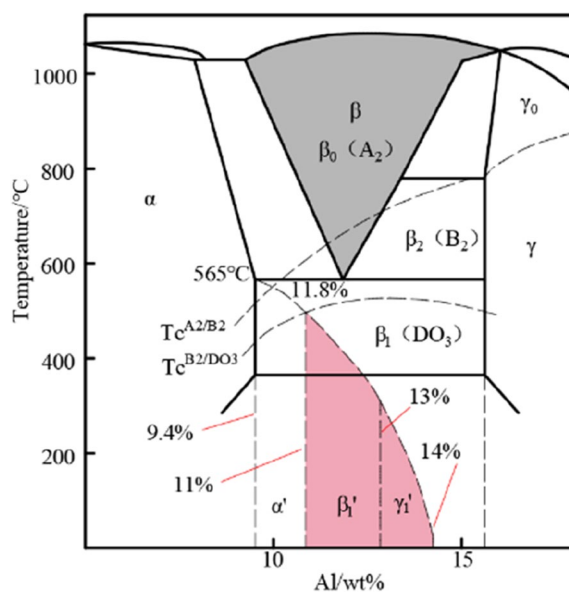


Figure 5: Binary phase diagram of Cu–Al system alloys.

to be 13 wt%, and the Fe content is used as a variable, with a range of 1–5 wt% and are referred to as 1Fe, 2Fe, 3Fe, 4Fe, and 5Fe alloys, respectively.

Alloy preparation

A circular tube method was used to prepare powder core wire materials for additive manufacturing, and the main preparation process is shown in Fig. 6. T2 copper tube with 99.9% purity, 4-mm outer diameter, and 0.7-mm wall thickness was selected as the outer skin of the powder core wire material, and the powder core was composed of Cu powder (325 mesh, purity: 99.9%), Al powder (200 mesh, purity: 99.9%), and Fe powder (300 mesh, purity: 99.8%). According to the alloy design composition, based on the “equal composition, equal volume” design principle [24], the prepared powder was filled into the circular tube of the powder core wire material by the vibration filling device after sufficient grinding. Then, the circular tube was drawn into 2.1-mm diameter wires under a customized integrated rolling and tapering device.

A thin-walled sample with a length of approximately 80 mm, a height of 10 mm, and a width of 5 mm was fabricated on the aluminum bronze substrate by fusion deposition using a RILAND RC-315SII AC/DC argon arc welding machine. The deposition process parameters were a deposition current of 140 A, a deposition velocity of 6 mm/s, and an argon gas flow rate of 10 L/min. An NSC-M332/W6 wire-cut EDM machine was used to cut a shape memory strip with dimensions of 65 × 3 × 1 mm from the center of the thin-walled wall fabricated by additive manufacturing, and several microstructure observation samples with thickness of 2.5 mm were cut along the deposition direction.

The heat treatment used in this study was divided into quenching heat treatment and recovery heat treatment after pre-deformation. The quenching process was carried out as follows: 950 °C × 2 h → 850 °C × 15 min → water quenching, with a heating and cooling rate of 15 °C/min. The shape memory strips and microstructure observation samples were quenched in the same batch. Recovery heat treatment after pre-deformation was performed by heating at a rate of 15 °C/min to the A_f (565 °C) + 50 °C of the Cu–Al alloy, holding for 10 min, and then removing and cooling in air.

Test method of SME

The shape memory properties of the alloy were tested using the bending deformation method as shown in Fig. 7. The pre-strain ε , elastic recovery (ER) ratio θ , and memory recovery (MR) ratio η of the alloy were calculated according to Eqs. (1, 2, and 3), respectively. To ensure the validity of the data, three parallel samples were prepared and measured for each composition

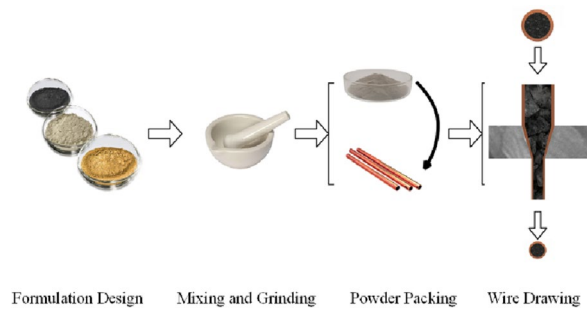


Figure 6: Flowchart of the preparation for the powder core wire.

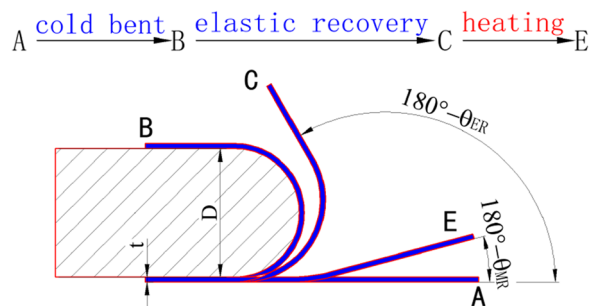


Figure 7: Schematic diagram for the shape recovery bending test.

and measured and their average values were used as the final results. The diameter of the mold used in this study was 24 mm ($D = 24$ mm), the height of the memory strip was 1 mm ($t = 1$ mm), and the pre-strain was calculated to be 4% according to Eq. (1).

$$\varepsilon = \frac{t}{D + t} \times 100\%, \quad (1)$$

$$\theta = \frac{\theta_{ER}}{180} \times 100\%, \quad (2)$$

$$\eta = \frac{\theta_{MR} - \theta_{ER}}{180 - \theta_{ER}} \times 100\%. \quad (3)$$

In the above equation, θ represents the elastic recovery ratio, θ_{ER} is the angle of free rebound, η represents the memory recovery ratio, and θ_{MR} is the angle of recovery after heating compared to bending at room temperature.

Analysis test method of microstructure

The prepared metallographic specimens were immersed in a solution of FeCl₃ hydrochloric acid for 3–10 s, rinsed with distilled water, and then immersed in anhydrous ethanol for ultrasonic cleaning. After drying, the specimens were observed with a CMY210 metallographic microscope.

Acknowledgments

This research did not receive any specific grant from funding agencies in the public, commercial, or not-for-profit sectors.

Author contributions

HW performed conceptualization, reviewing, editing of the manuscript, and supervision. JF contributed to conceptualization, investigation, and writing of the manuscript. SC performed writing and editing of the manuscript and visualization. XY performed reviewing and supervision. DX performed validation and supervision.

Data availability

The data that support the findings of this study are available on request from the corresponding author.

Declarations

Conflict of interest There is no conflict of interest to disclose.

Ethical approval

Not applicable.

References

1. R. Dasgupta, A look into Cu-based shape memory alloys: present scenario and future prospects. *J. Mater. Res.* **29**, 1681–1698 (2014)
2. J.M. Jani, M. Leary, A. Subic, M.A. Gibson, A review of shape memory alloy research, applications and opportunities. *Mater. Des.* **1980–2015**(56), 1078–1113 (2014)
3. E.M. Mazzer, M.R. da Silva, P. Gargarella, Revisiting Cu-based shape memory alloys: recent developments and new perspectives. *J. Mater. Res.* **37**, 162–182 (2022)
4. P.S. Yao, H.Y. Huang, Y.J. Su, J.X. Xie, Two-way shape memory effect induced by tensile deformation in columnar-grained Cu_{71.7}Al_{18.1}Mn_{10.2} alloy. *Materials* **11**(11), 2109 (2018)
5. X. Lu, F. Chen, W. Li, Y. Zheng, Effect of Ce addition on the microstructure and damping properties of Cu–Al–Mn shape memory alloys. *J. Alloys Compd.* **480**, 608–611 (2009)
6. D.V. Kudashov, R. Zauter, H.R. Müller, Spray-formed high-aluminium bronzes. *Mater. Sci. Eng., A* **477**, 43–49 (2008)
7. S.M. Ueland, Y. Chen, C.A. Schuh, Oligocrystalline shape memory alloys. *Adv. Func. Mater.* **22**(10), 2094–2099 (2012)
8. A. Agrawal, S.K. Vajpai, Preparation of Cu–Al–Ni shape memory alloy strips by spray deposition-hot rolling route. *Mater. Sci. Technol.* **36**, 1337–1348 (2020)
9. J. Liu, M. Li, X. Li, W. Yan, W. Huang, S. Yan, The effect of superelastic strain on the damping capacity in columnar-grained Cu–Al–Mn shape memory alloy. *J. Alloy. Compd.* **781**, 621–628 (2019)
10. B.N. Guniputi, S.M. Murigendrappa, Influence of Gd on the microstructure, mechanical and shape memory properties of Cu–Al–Be polycrystalline shape memory alloy. *Mater. Sci. Eng. A* **737**, 245–252 (2018)
11. Xu. Duo et al., Comparison of shape memory properties between Cu–12.5 Al–3Mn and Cu–12.5 Al–3Mn–1Ni produced by additive manufacturing technology. *J. Mater. Res. Technol.* (2023). <https://doi.org/10.1016/j.jmrt.2023.08.136>
12. L. Guo, F. Chen, S. Chen, Y. Huang, J. Zhang, C. Wang, S. Yang, The improvement of the shape memory effect of Cu–135 Al–4Ni high-temperature shape memory alloys through Cr-, Mo-, or V-alloying. *J. Sci.: Adv. Mater. Dev.* **8**(2), 100532 (2023)
13. S. Vajpai, R. Dube, S. Sangal, Application of rapid solidification powder metallurgy processing to prepare Cu–Al–Ni high temperature shape memory alloy strips with high strength and high ductility. *Mater. Sci. Eng. A* **570**, 32–42 (2013)
14. S.Y. Yang, F. Zhang, J.L. Wu, J.B. Zhang, C.P. Wang, X.J. Liu, Microstructure characterization, stress–strain behavior, super-elasticity and shape memory effect of Cu–Al–Mn–Cr shape memory alloys. *J. Mater. Sci.* **52**, 5917–5927 (2017)
15. S.Y. Yang, Y. Su, C.P. Wang, X.J. Liu, Microstructure and properties of Cu–Al–Fe high-temperature shape memory alloys. *Mater. Sci. Eng. B* **185**, 67–73 (2014)
16. S.Y. Yang, T. Omori, C.P. Wang et al., A jumping shape memory alloy under heat. *Sci. Rep.* **6**, 1–6 (2016)
17. E. Aldirmaz, M. Güler, E. Güler, Effect of nickel addition on the magnetic and microstructural properties of Cu–Al–Fe Alloy. *J. Supercond. Novel Magn.* **33**, 755–759 (2020)
18. T. Raju, V. Sampath, Effect of ternary addition of iron on shape memory characteristics of Cu–Al alloys. *J. Mater. Eng. Perform.* **20**, 767–770 (2011)
19. H.Y. Wang, J.L. Huang et al., Comparison of microstructure and shape memory properties between two Cu–Al–Mn alloys produced by additive manufacturing technology. *Materialia* **26**, 101594 (2022)
20. L. Wang, *Study on the solidification structure and properties of Cu–Fe alloy* (Northeastern University, Boston, 2010)
21. H.Y. Wang, J.L. Huang et al., Microstructure and shape memory properties of Cu–Al–Fe alloys with different Al contents made by additive manufacturing technology. *Mater. Res. Express.* **9**, 095701 (2022)
22. J. Yang, P. Ouyang, T. Liu et al., First-principles study of the effect of aluminum content on the elastic properties of Cu–Al alloys. *Mater. Today Commun.* **31**, 103399 (2022)
23. Joint Writing Group for Casting Nonferrous Alloys and Their Melting, *Casting non-ferrous alloys and their melting* (Defense Industry Press, Arlington, 1980)

24. Wang et al., Functional low-loss shape memory alloy micro-nano powder core wire material for laser additive manufacturing, WO2019223083 (2019)

Publisher's Note Springer Nature remains neutral with regard to jurisdictional claims in published maps and institutional affiliations.

Springer Nature or its licensor (e.g. a society or other partner) holds exclusive rights to this article under a publishing agreement with the author(s) or other rightsholder(s); author self-archiving of the accepted manuscript version of this article is solely governed by the terms of such publishing agreement and applicable law.